Controlling the Dual-Emission Character of Aryl-Modified *o*-Carboranes by Intramolecular CH···O Interaction Sites

Mr. Junki Ochi, Mr. Kazuhiro Yuhara, Prof. Kazuo Tanaka* and Prof. Yoshiki Chujo

Department of Polymer Chemistry, Graduate School of Engineering, Kyoto University Katsura, Nishikyo-ku, Kyoto 615-8510, Japan

E-mail: tanaka@poly.synchem.kyoto-u.ac.jp

Abstract

It is still challenging to realize the dual-emission system, in which two luminescent bands simultaneously appear by the photo excitation, in solid with organic dyes due to difficulty in regulation of electronic properties in the excited state and concentration quenching. *o*-Carborane is known to be a versatile platform for constructing solid-state emitters since the sphere boron cluster is favorable for suppressing intermolecular interactions and subsequently concentration quenching. In this paper, we show the solid-state dual-emissive *o*-carborane derivatives. We prepared 4 types of *o*-carborane derivatives and found dual-emission behaviors both in solution and solid states. By regulating rotation at the *o*-carborane unit with the intramolecular $C_{cage}H\cdots O$ interaction, intensity ratios in dual emission were changed. Finally, it was demonstrated that the overall photoluminescence spectra can be estimated by the binding energy of intramolecular interactions.

Introduction

The dual-emissive systems, which can simultaneously show two distinct PL bands by photo-excitation, attract great attention as a platform for developing organic optoelectric devices and sensors.[1] For example, their bimodal PL bands covering a wide range of the visible region are favorable for realizing white-light emission.[2] By chemical modification, it is easy to tune color balances in these materials. In the biotechnology field, dual-emission behaviors are useful for designing a precise sensing probe. From the changes in intensity ratios between two emission bands, it is possible to quantify the degree of alteration of environmental parameters and target concentrations.[3] Owing to environmental sensitivity of excited molecules, slight changes can be monitored by such ratiometric probes. For realizing the dual-emission behaviors, the coexistence of two excited states is the major strategy.[1] By simultaneously observing the combinational emission bands with the transitions from the locally-excited (LE) state and the triplet-excited state (phosphorescence)[4] or twisted intramolecular charge transfer (TICT),[5] dual emission can be obtained. Additionally, anti-Kasha emission[6] and emission from and excited-state intramolecular proton transfer (ESIPT)[7] are also available for dual-emission systems. To obtain desired properties, it is of great significance to restrict transition with some extent from the LE to another excited state. In the solution state, such precise control of the transition in the excited state is applicable, whereas it is challenging in solid due to structural entanglement in the condensed state and concentration quenching.

o-Carborane (1,2-dicarba-*closo*-dodecaborane, $C_2B_{10}H_{12}$) is one promising scaffold as dual emission materials.[8,9] In aryl-substituted *o*-carboranes, the parallel conformation where the dihedral angle (φ) of the C–C bond in the *o*-carborane unit toward the π-plane of the aryl moiety is 0° is generally stable. On the other hand, the perpendicular conformation between the C–C bond and π-plane is more stable in the excited state originating from electronic

communication, such as exo-π-interaction,[10] between *o*-carborane and the aryl group.[11–13] Driven by this stabilization gain, intramolecular rotation occurs after photoexcitation, followed by the formation of the intramolecular charge transfer (ICT) state.[14,15] As a result, intense emission with the ICT character appeared.[16] Interestingly, intramolecular rotation followed by the formation of the ICT state can be observed even in the solid state. Moreover, because of steric hindrance of *o*-carborane units, intermolecular interaction can be effectively disturbed. As a result, solid-state luminescence with the ICT character can be exhibited.

By suppressing intramolecular rotation in the excited state, dual-emission systems consisted of LE and ICT emission bands can be realized with aryl-modified *o*-carborane derivatives. One outstanding dual emission material is the single-molecule white light emitter reported by Yan and coworkers.[17] High emission efficiency (67%) was detected even in the solid state.[17] As another examples, the reversible mechanochromic luminescence caused by the appearance/disapperance of the ICT band was accomplished.[18,19] Our group also reported that the triaryl-substituted *o*-carborane derivative can show white-light emission in the specific aggregation state.[20] More recently, we reported thermochromic luminescent behaviors of bis(thienylethynyl)benzene-based *o*-carborane in amorphous polystyrene films.[21] By the aggregation formation of *o*-carborane species in polymer matrices, luminescent chromic behaviors originating from the enhancement of ICT emission were observed. Although the changes in intensity ratio were slight, clear luminescent chromic behaviors can be exhibited owing to dual-luminescent nature. By introducing substituents and cooling, the LE emission can be induced.[22–24] Similarly to the previous examples, changes in the degree of intramolecular rotation should be responsible for dual-emission properties. However, it is still challenging to tune dual-luminescent properties according to the programmed design due to difficulty in the regulation of intramolecular rotation.

Herein, we demonstrate the new strategy to control the dual emission character of aryl-*o*-carboranes by introducing an intramolecular interaction site. The key feature is the weak acidic hydrogen atom on the cage-carbon atom ($C_{cage}H$), which can form noncovalent interactions with electron-rich atoms.[25] We have recently shed light on this unique interaction to construct solid-state thermochromic materials possessing the highly-ordered crystal structures assisted by intermolecular $C_{cage}H\cdots N$ interactions.[26,27] On the other hand, intramolecular interactions have not been sufficiently investigated except for pioneering works conducted by Endo and coworkers.[28] Those researches focused on 1-(methoxyphenyl)-*o*-carborane and the intramolecular $C_{cage}H\cdots O$ interaction was evaluated by the NMR spectroscopy and the quantum chemical calculation, while optical properties have not been investigated because of its small π-conjugation. Based on this work, we newly introduced larger π-planes possessing intramolecular interaction sites into the *o*-carborane scaffold. The interactions affected φ values both in solution and solid states, and LE/ICT balance was drastically changed as shown below.

Results and Discussion

Syntheses of the target oxygen-containing *o*-carboranes are shown in Scheme 1. In addition to $C_{cage}H\cdots O$ interacted systems **H-OMe** and **H-DBF**, the corresponding model compounds **Me-OMe** and **Me-DBF** without the $C_{cage}H$ atom were prepared. First, the desired alkynes **3–6** were obtained through the Sonogashira-type coupling reaction[29] from **1** or **2**. The following reaction with $B_{10}H_{12}(CH_3CN)_2$ catalyzed by the previously reported silver complex[30] afforded the corresponding compounds, **H-OMe**, **Me-OMe**, **H-DBF**, and **Me-DBF**, although the reaction yields were low probably because of steric hindrance of the substituents.[22] The products were characterized by ^{1}H and $^{13}C\{^{1}H\}$ NMR spectroscopy and high-resolution mass spectrometry. Final products containing the *o*-carborane unit were also characterized by ^{11}B NMR spectroscopy and single-crystal X-ray crystallography.

(Scheme 1)

Single crystal X-ray analyses revealed formation of intramolecular $C_{cage}H\cdots O$ interactions in **H-OMe** and **H-DBF** (Figure 1). In these compounds, the $C_{cage}H$ and oxygen atoms were closely arranged (2.07 Å for **H-OMe** and 2.16 Å for **H-DBF**), and the dihedral angles $\varphi_{C2\text{-}C1\text{-}C3\text{-}C4}$ were nearly planar (–16.8(8)° for **H-OMe** and 0.0° for **H-DBF**). The geometrically more crowded environment around $C_{cage}H\cdots O$ atoms of **H-OMe** caused slight torsion of the aromatic ring, while **H-DBF** was perfectly planar. In the case of methylated analogs **Me-OMe** and **Me-DBF**, steric hindrance of the methyl group preferred perpendicular orientation with large $\varphi_{C2\text{-}C1\text{-}C3\text{-}C4}$ values (–92.3(4)° for **Me-OMe** and –89.6(3)° for **Me-DBF**). These results suggest that intramolecular $C_{cage}H\cdots O$ interactions can effectively regulate the molecular orientation in the crystalline state.

(Figure 1)

From spectroscopic data and computational calculations, the degree of the $C_{cage}H\cdots O$ interaction in **H-OMe** than **H-DBF** was estimated. First, the ^1H NMR signals of the $C_{cage}H$ atom were monitored in various solvents (Table 1). It was reported that strong intermolecular interaction between the $C_{cage}H$ and solvent atoms induces large degree of signal peak shifts in the spectra.[28] Therefore, we evaluated the magnitude of interaction as a width of peak shift ranges (Δppm). The signal peaks of the pristine *o*-carborane were observed from 4.89 (in DMSO-d_6) to 2.02 (in C_6D_6) ppm. Although similar solvent dependency was observed from **H-OMe** and **H-DBF**, the Δppm values were much smaller than that of *o*-carborane (Table 1), meaning that the intermolecular interactions with solvents should be smaller in **H-OMe** and **H-DBF**. In particular, Δppm from **H-OMe** was the smallest of the three. Intramolecular interaction should prevent from intermolecular ones with solvent molecules, and **H-OMe** can form stronger interaction than **H-DBF**. This speculation is supported by the fact that previously reported 1-(2-methoxyphenyl)-*o*-carborane, which can form intramolecular interaction, also showed the close Δppm value 0.77.[28] Next, interactions in the solid state were investigated by infrared spectroscopy (Figure S8). The peak assigned as the C_{cage}–H stretching band shifted to the larger energy region, suggesting the formation of CH···O interaction. Although general hydrogen bonds shift the band to a smaller energy region,[26] the opposite shift is also known as an "improper hydrogen bond," which is sometimes observed in CH···X hydrogen bonding systems.[31] From these results, the $C_{cage}H\cdots O$ interaction should be formed both in solution and solid states. Finally, atoms-in-molecules (AIM) analysis[32] was conducted to estimate $C_{cage}H\cdots O$ binding energies. Emamian and coworkers recently proposed that electron density at the bond critical point (ρ_{BCP}) showed good correlation with binding energy (BE), namely, BE (kcal/mol) = $-223.08 \times \rho_{BCP}$ (a.u.) + 0.7423

for neutral complexes.[33] The estimated BE values were 5.22 kcal/mol for **H-OMe** and 3.68 kcal/mol for **H-DBF** in the crystalline state, showing good agreement with ^{1}H NMR analyses. Thus, it is concluded that **H-OMe** involves the stronger $C_{cage}H\cdots O$ interaction than **H-DBF** both in the solution and crystalline states.

(Table 1)

The ICT character was confirmed by the solvatochromicity of each emission band. Accordingly, the obvious solvatochromic shift was observed from the emission bands in the longer wavelength regions with the solutions containing **Me-OMe** and **Me-DBF**, while the emission bands in the shorter wavelength regions were inert to solvent polarity (Figures S3 and S4). These data indicate that the emission bands in shorter and longer wavelength region are attributable to LE and ICT emission, respectively. Based on these assignment, it was revealed from optical measurements in the diluted solutions (CH_2Cl_2, 1.0×10^{-5} M) that the intramolecular $C_{cage}H\cdots O$ interactions should impact on PL properties (Figure 2 and Table 2). From **H-OMe** and **H-DBF**, their PL spectra were dominated by LE emission originated from 9-methoxyphenanthorene (Figure S5) or dibenzofurane.[34] Due to small $\varphi_{C2\text{-}C1\text{-}C3\text{-}C4}$ values, the formation of the ICT state should be restricted in the excited state. Meanwhile, **Me-OMe** and **Me-DBF** having large $\varphi_{C2\text{-}C1\text{-}C3\text{-}C4}$ values exhibited characteristic ICT emission bands around 500–700 nm. Significant electronic interaction between the aromatic moiety and *o*-carborane in the perpendicular conformations can encourage the formation of the ICT state. Note that UV–vis absorption spectra mainly reflected the π–π^* transition character of the aromatic moiety, and the intramolecular $C_{cage}H\cdots O$ interaction hardly influence on the absorption spectra except for slight spectral shift originated from the electron-donating ability of the methyl group (Figure S2).[16]

(Figure 2 and Table 2)

PL spectra from the solid samples of aryl-modified *o*-carboranes can be classified into three types in terms of LE/ICT balance; 1) LE dominant (**H-OMe**), 2) LE/ICT dual-emissive (**H-DBF**), and 3) ICT dominant (**Me-OMe** and **Me-DBF**). Most of previous aryl-*o*-carboranes are categolized in type 3 in which the ICT emission band tends to be drastically enhanced by aggregation or crystallization.[8,35] Even if the $\varphi_{C2\text{-}C1\text{-}C3\text{-}C4}$ values are small in the single crystal structure, owing to the globular structure of *o*-carborane, the rotary motion around C1–C3 bond can occur to form the energetically favored ICT state after photoexcitation.[11] In contrast, the LE emission bands of **H-OMe** and **H-DBF** survived even in the solid state, implying that the formation of ICT state might be restricted. The stronger interaction in **H-OMe** plays a critical role in the disturbance of molecular rotation followed by the formation of the ICT state, while LE and ICT states can be simultaneously realized because of the moderate anchoring of rotation in **H-DBF**. In more detail, the **H-DBF** solid sample showed the additional shoulder peak around 500 nm. This band could be attributable to PL from aggregates because photoexcitation at 365 nm where **H-DBF** has no absorption generated the similar band around 500 nm (Figure S7). Moderate degree of π-stacking in the single-crystal structure of **H-DBF** supported this assignment (Figure S1). From these data, it is clearly shown that the solid-state luminescence with the LE character can be obtained from aryl-*o*-carborane crystals, and especially intensity of LE emission can be modulated by regulating the degree of intramolecular interaction. In other words, LE/ICT balance can be tuned by the intramolecular $C_{cage}H\cdots O$ interaction strength.

The quantum calculations supported LE and ICT characters of the synthesized compounds (Figure 3). First, the isolated molecules were structurally optimized both in S_0 and S_1 states. In the S_1 states of **H-OMe** and **H-DBF**, two optimized structures ES(LE) and ES(ICT) with different $\varphi_{C2\text{-}C1\text{-}C3\text{-}C4}$ values were obtained, which respectively corresponds to the LE and ICT state. **Me-OMe** and **Me-DBF** afforded only ES(ICT) geometry because of the steric methyl group. Transitions between S_0 and S_1 states were mainly dominated by the highest occupied molecular orbital (HOMO) and the lowest unoccupied molecular orbital (LUMO), as shown in Tables S17–S26. In the S_1(LE)–S_0 transitions, both HOMO and LUMO were mainly localized on the aromatic unit. On the other hand, in the S_1(ICT)–S_0 transitions, LUMO was on the *o*-carborane unit, and HOMO was on the aromatic unit, indicating the ICT character of this transition. The oscillator strength *f* in S_1(ICT)-S_0 transition depended on the Ar group; the phenanthrene series had large *f* (0.1700 for **H-OMe** and 0.1677 for **Me-OMe**), and the dibenzofuran series had small ones (0.0073 for **H-DBF** and 0.0084 for **Me-DBF**). On the other hand, the experimental PL spectra showed that ICT emission was more dominant in **H-DBF** than **H-OMe**. This could not be rationalized by their *f* values but more blocked ICT formation in **H-OMe** by the stronger $C_{cage}H\cdots O$ interaction. These results again emphasized the significant impact of intramolecular $C_{cage}H\cdots O$ interactions on the PL spectra.

In Figure 2 and Table 2, the ICT emission bands in the CH_2Cl_2 solution were drastically blue-shifted to those in solid in **Me-OMe** (580 nm → 519 nm) and **Me-DBF** (550 nm → 457 nm). This phenomenon has also been reported in other methylated *o*-carboranes.[16,24] To gain insight on this blue-shift, QM/MM calculations using the single-crystal structures of **Me-OMe** and **Me-DBF** were conducted. Accordingly, we obtained larger S_1–S_0 transition energy values from the solid state compared to the isolated single molecule (Tables S27 and S28). Moreover, such large blue-shift was not obtained in **H-DBF** (Tables S29 and S30) corresponding with the experimental spectra. These results suggest that methyl group should

inhibit the structural relaxation after photoexcitation in the crystalline packing, exhibiting blue-shifted PL spectra from those in the solutions.

(Figure 3)

A temperature-responsive property of the intramolecular $C_{cage}H\cdots O$ interaction site is demonstrated. PL spectra of **H-OMe** and **H-DBF** were collected with the solid samples between 80 K and 440 K. The overall PL intensity gradually decreased in the relatively-higher temperature region in both samples (Figure 4, left column). The normalized spectra with the LE emission intensity revealed the consecutive change of LE/ICT emission ratio (Figure 4, right column). ICT emission got dominant in the higher temperature region because of the activated rotary motions around the C_{cage}–Ar bond.[24] Although the spectrum of **H-DBF** was more complex than that of **H-OMe** due to the abovementioned third PL band around 500 nm, the overall trend was similar. On the other hand, **Me-OMe** and **Me-DBF** showed monotonous decrease of the ICT band as the temperature rose (Figure S6). These results clearly suggest that modulation of intramolecular rotations should be a key component for designing stimuli-responsive dual emitters based on the *o*-carborane scaffold.

Conclusion

To regulate the dual emission property of aryl-*o*-carboranes, we newly employed intramolecular $C_{cage}H\cdots O$ interaction sites. From the structural analyses and computer calculations, it was shown that the molecular distribution between the C_{cage}–C_{cage} bond and the π-plane can be tuned both in the solution and solid states. Although most previously-reported aryl-modified *o*-carboranes showed ICT-dominant PL spectra, the planarly locked structures suppressed the effective ICT pathways and realized a balanced LE/ICT ratio. Moreover, the ICT efficiency was able to be regulated by tuning the binding energy of interaction sites. Methyl-substituted model compounds showed only ICT emission in contrast to intramolecular interacted systems, revealing a strong correlation between the molecular structure and the PL spectrum. Our results described here can open the rational strategy for controlling the dual emission property based on excitation-driven movable molecules, such as *o*-carborane and can prove the great potential of this compound as an "element-block"[36–39] for the intuitive design of dual emission materials.

Experimental Section

Experimental procedures and further analytical data of new compounds are described in the Supporting Information.

Deposition Number(s) <url href="https://www.ccdc.cam.ac.uk/services/structures?id=doi:10.1002/chem.202200155"> 2132594 (for **H-OMe**), 2132597 (for **Me-OMe**), 2132598 (for **H-DBF**), 2132599 (for **Me-DBF**)</url> contain(s) the supplementary crystallographic data for this paper. These data are provided free of charge by the joint Cambridge Crystallographic Data Centre and

Fachinformationszentrum Karlsruhe <url href=" http://www.ccdc.cam.ac.uk/structures ">Access Structures service</url>.

ACKNOWLEDGMENT

This work was partially supported by the Nakatani Foundation (for K.T.) and JSPS KAKENHI Grant Numbers JP21H02001 and JP21K19002 (for K.T) and JP21J14940 (for J.O).

Keywords

Carboranes; Dual emission; Fluorescence; Hydrogen bonds; Thermochromic luminescence

References

[1] S. K. Behera, S. Y. Park, J. Gierschner, *Angew. Chem. Int. Ed.* **2021**, *60*, 22624–22638.

[2] Z. Chen, C. Ho, L. Wang, W. Wong, *Adv. Mater.* **2020**, *32*, 1903269.

[3] M. H. Lee, J. S. Kim, J. L. Sessler, *Chem. Soc. Rev.* **2015**, *44*, 4185–4191.

[4] M. Shimizu, S. Nagano, T. Kinoshita, *Chem. - Eur. J.* **2020**, *26*, 5162–5167.

[5] Z. R. Grabowski, K. Rotkiewicz, W. Rettig, *Chem. Rev.* **2003**, *103*, 3899–4032.

[6] T. Itoh, *Chem. Rev.* **2012**, *112*, 4541–4568.

[7] V. S. Padalkar, S. Seki, *Chem. Soc. Rev.* **2016**, *45*, 169–202.

[8] J. Ochi, K. Tanaka, Y. Chujo, *Angew. Chem. Int. Ed.* **2020**, *59*, 9841–9855.

[9] R. Núñez, M. Tarrés, A. Ferrer-Ugalde, F. F. de Biani, F. Teixidor, *Chem. Rev.* **2016**, *116*, 14307–14378.

[10] C. H. Ryu, S. H. Lee, S. Yi, J. H. Hong, S. Im, K. M. Lee, *Eur. J. Inorg. Chem.* **2021**, *2021*, 4875–4881.

[11] H. Naito, K. Nishino, Y. Morisaki, K. Tanaka, Y. Chujo, *Angew. Chem. Int. Ed.* **2017**, *56*, 254–259.

[12] L. Weber, J. Kahlert, R. Brockhinke, L. Böhling, A. Brockhinke, H. Stammler, B. Neumann, R. A. Harder, M. A. Fox, *Chem. – Eur. J.* **2012**, *18*, 8347–8357.

[13] J. Ochi, K. Tanaka, Y. Chujo, *Dalton Trans.* **2021**, *50*, 1025–1033.

[14] K. L. Martin, A. Krishnamurthy, J. Strahan, E. R. Young, K. R. Carter, *J. Phys. Chem. A* **2019**, *123*, 1701–1709.

[15] S. Kwon, K.-R. Wee, Y.-J. Cho, S. O. Kang, *Chem. - Eur. J.* **2014**, *20*, 5953–5960.

[16] H. Naito, K. Nishino, Y. Morisaki, K. Tanaka, Y. Chujo, *J. Mater. Chem. C* **2017**, *5*, 10047–10054.

[17] D. Tu, P. Leong, S. Guo, H. Yan, C. Lu, Q. Zhao, *Angew. Chem. Int. Ed.* **2017**, *56*, 11370–11374.

[18] X. Wu, J. Guo, Y. Cao, J. Zhao, W. Jia, Y. Chen, D. Jia, *Chem. Sci.* **2018**, *9*, 5270–5277.

[19] D. Tu, P. Leong, Z. Li, R. Hu, C. Shi, K. Y. Zhang, H. Yan, Q. Zhao, *Chem. Commun.* **2016**, *52*, 12494–12497.

[20] M. Tominaga, H. Naito, Y. Morisaki, Y. Chujo, *New J. Chem.* **2014**, *38*, 5686–5690.

[21] K. Wada, K. Hashimoto, J. Ochi, K. Tanaka, Y. Chujo, *Aggregate* **2021**, *2*, e93.

[22] K. Nishino, K. Tanaka, Y. Chujo, *Asian J. Org. Chem.* **2019**, *8*, 2228–2232.

[23] H. Mori, K. Nishino, K. Wada, Y. Morisaki, K. Tanaka, Y. Chujo, *Mater. Chem. Front.* **2018**, *2*, 573–579.

[24] K. Nishino, H. Yamamoto, K. Tanaka, Y. Chujo, *Org. Lett.* **2016**, *18*, 4064–4067.

[25] M. Fox, *Coord. Chem. Rev.* **2004**, *248*, 457–476.

[26] J. Ochi, K. Tanaka, Y. Chujo, *Inorg. Chem.* **2021**, *60*, 8990–8997.

[27] J. Ochi, K. Tanaka, Y. Chujo, *Eur. J. Org. Chem.* **2019**, *2019*, 2984–2988.

[28] K. Ohta, H. Yamazaki, F. Pichierri, M. Kawahata, K. Yamaguchi, Y. Endo, *Tetrahedron* **2007**, *63*, 12160–12165.

[29] J. Moon, M. Jang, S. Lee, *J. Org. Chem.* **2009**, *74*, 1403–1406.

[30] M. E. El-Zaria, K. Keskar, A. R. Genady, J. A. Ioppolo, J. McNulty, J. F. Valliant, *Angew. Chem. Int. Ed.* **2014**, *53*, 5156–5160.

[31] F. Ito, *J. Chem. Phys.* **2012**, *137*, 014505.

[32] Bader, R. F. W. in *Atoms in Molecules: A Quantum Theory*, Clarendon Press, **1994**.

[33] S. Emamian, T. Lu, H. Kruse, H. Emamian, *J. Comput. Chem.* **2019**, *40*, 2868–2881.

[34] N. Rajendiran, R. K. Sankaranarayanan, G. Venkatesh, *Bull. Chem. Soc. Jpn.* **2014**, *87*, 797–808.

[35] H. Yamamoto, J. Ochi, K. Yuhara, K. Tanaka, Y. Chujo, *Cell Rep. Phys. Sci*. **2022**, DOI: 10.1016/j.xcrp.2022.100758.

[36] K. Tanaka, Y. Chujo, *Polym. J.* **2020**, *52*, 555–566.

[37] M. Gon, K. Tanaka, Y. Chujo, *Bull. Chem. Soc. Jpn.* **2019**, *92*, 7–18.

[38] M. Gon, K. Tanaka, Y. Chujo, *Polym. J.* **2018**, *50*, 109–126.

[39] Y. Chujo, K. Tanaka, *Bull. Chem. Soc. Jpn.* **2015**, *88*, 633–643.

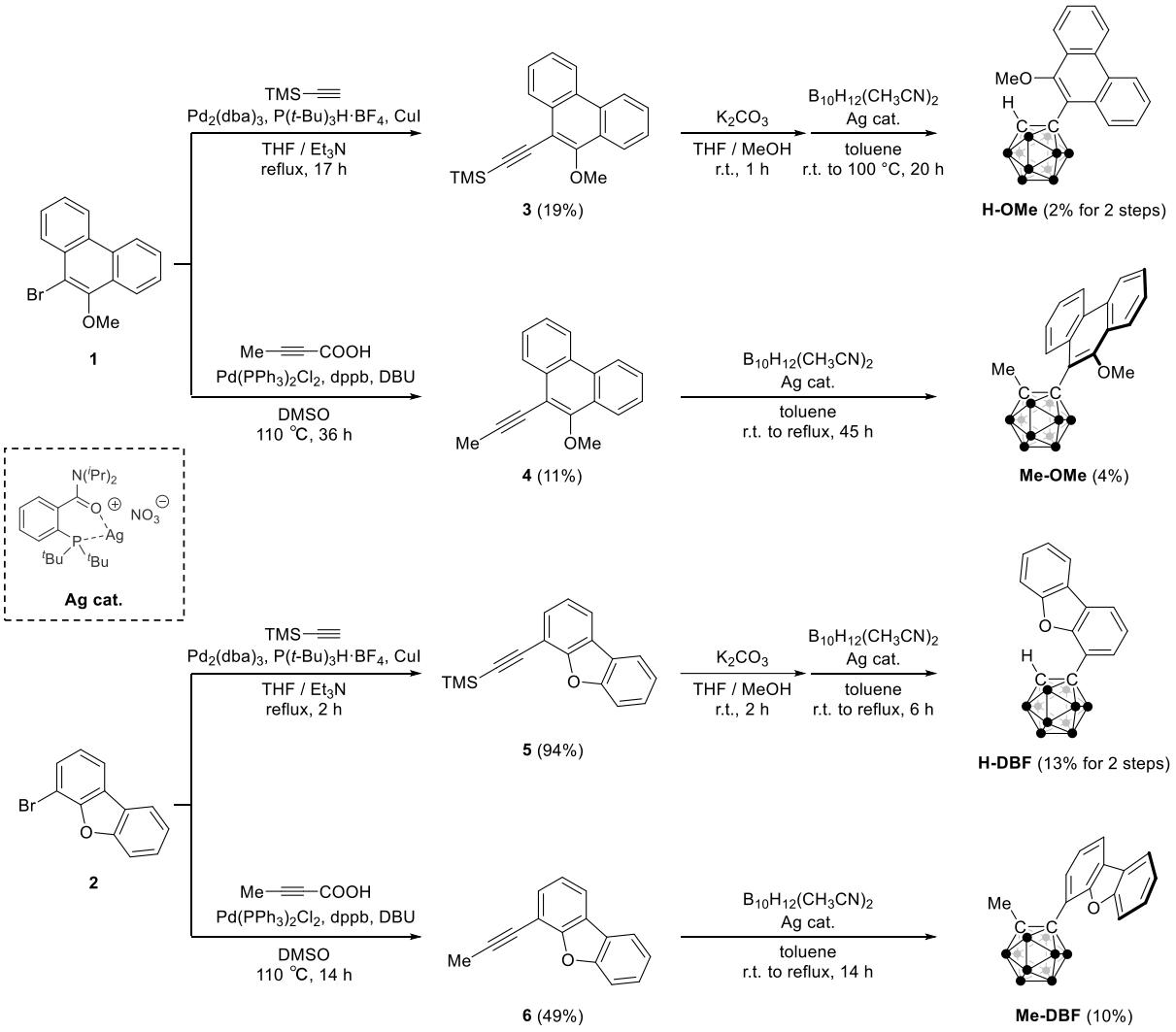

Scheme 1. The synthetic routes of oxgen-containing target molecules.

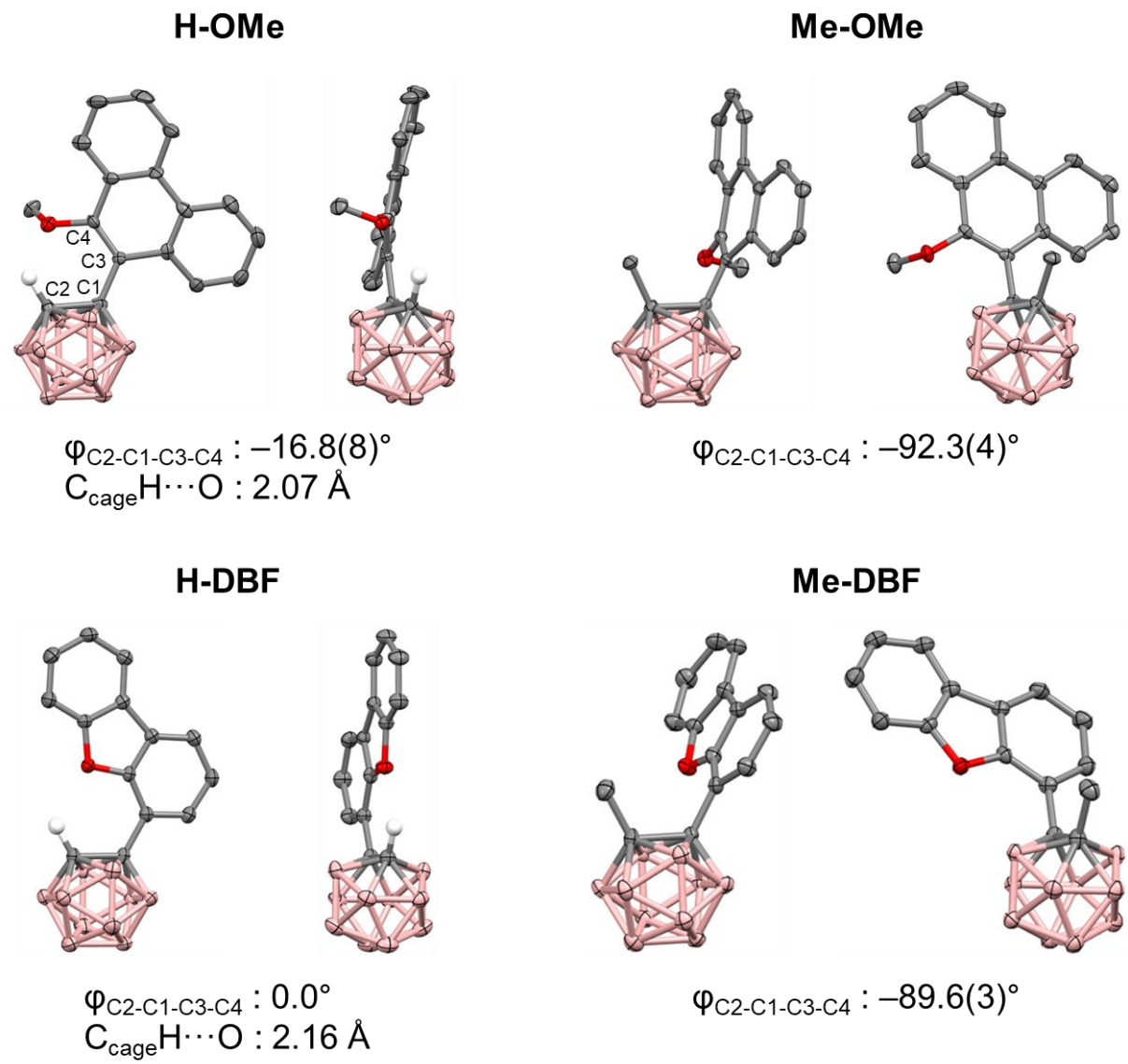

Figure 1. Single-crystal structures of the synthesized compounds.

Table 1. Summarized ^{1}H NMR chemical shift values of the $C_{cage}H$ atom in various solvents

Solvent	Chemical shift of the $C_{cage}H$ atom (ppm)				
	o-Carborane	1-Ph-*o*-Carborane[28]	**H-DBF**	**H-OMe**	1-(2-OMePh)-*o*-Carborane[28]
DMSO-d_6	4.89	5.79	6.17	6.57	5.98
CD_3OD	4.31	5.09	5.83	6.46	5.67
CD_3CN	4.05	4.67	5.81	6.45	5.71
$CDCl_3$	3.55	3.97	5.49	6.21	5.36
C_6D_6	2.02	2.92	5.10	6.02	5.22
Δppm	**2.87**	**2.87**	**1.07**	**0.55**	**0.76**

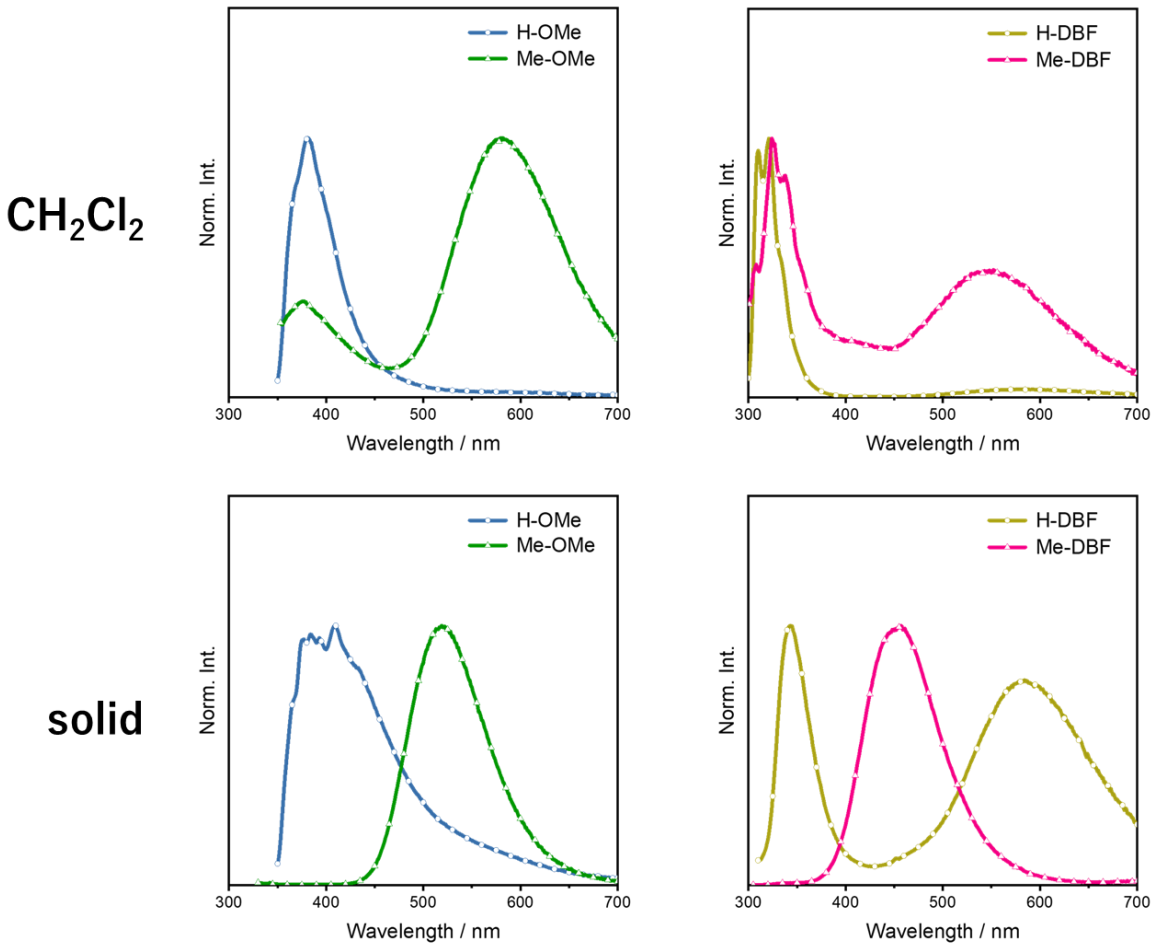

Figure 2. PL spectra of the synthesized compounds in CH_2Cl_2 (1.0×10^{-5} M) (top) and in solid (bottom).

Table 2. Photophysical properties of the synthesized compounds

Compound	1.0×10^{-5} M CH_2Cl_2 solution				solid		
	λ_{max}^{abs} / nm	λ_{max}^{PL} / nm	τ / ns	Φ_{PL}	λ_{max}^{PL} / nm	τ / ns	Φ_{PL}
H-OMe	262/304	381	7.3	< 0.01 (LE)	410	6.3 (4%) 1.3 (96%)	0.02 (LE)
Me-OMe	264	377/580	8.2 (27%) 2.2 (73%)	0.02 (LE & ICT)	519	7.7 (17%) 5.0 (83%)	0.87 (ICT)
H-DBF	254/286	321/584	3.8	0.01 (LE)	343/584	3.0	0.04 (LE & ICT)
Me-DBF	290	324/550	2.1	0.01 (LE & ICT)	457	2.7	0.02 (ICT)

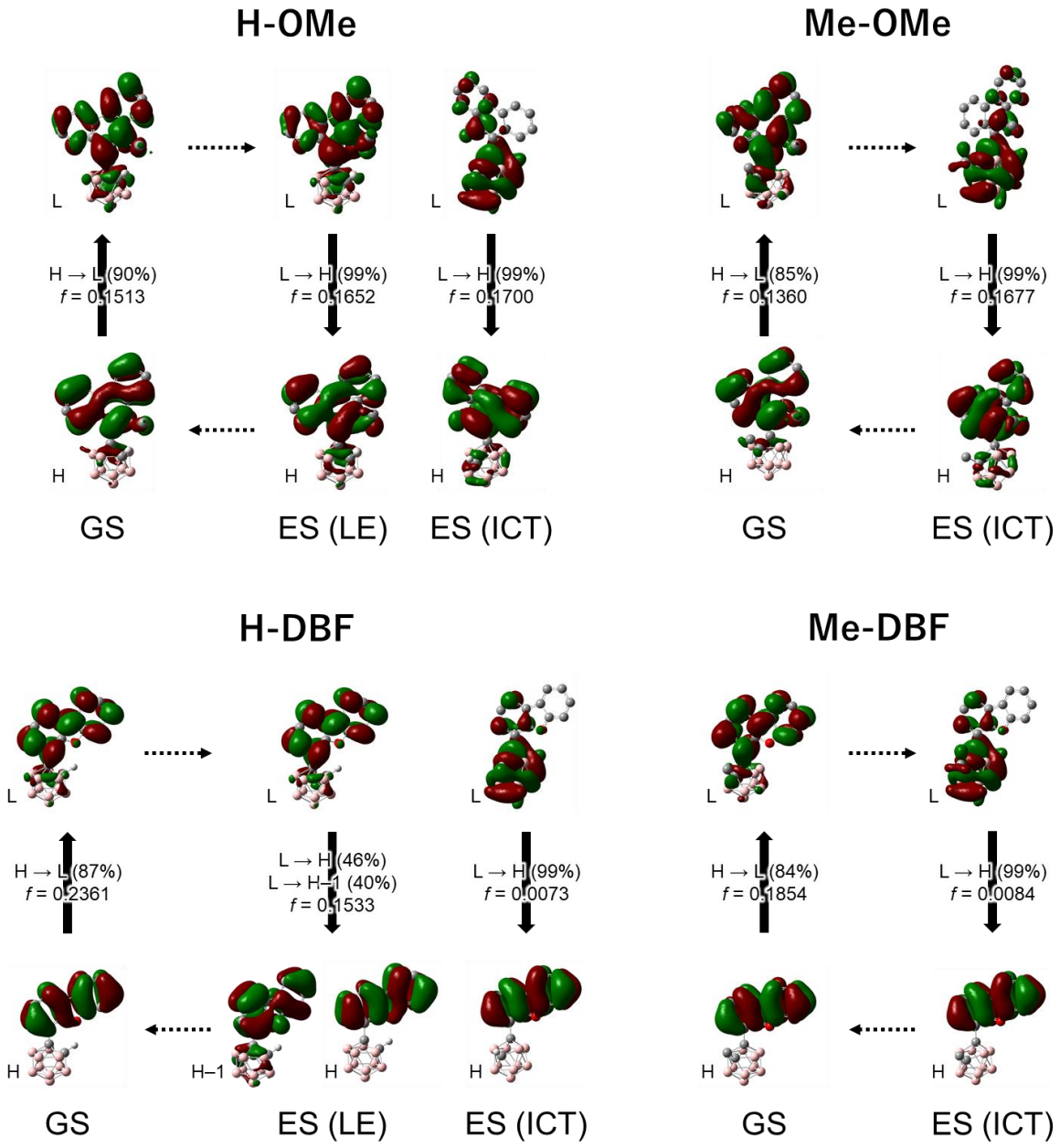

Figure 3. Characters of main electronic transitions of the synthesized compounds obtained by B3LYP/6-31G+(d,p) level. H…HOMO, L…LUMO, GS…ground state, ES…exsited state. Transitions at GS in this figure correspond to the S_0–S_2 transitions considering the forbidden character of the S_0–S_1 transitions (Tables S17-S26). Transitions at ES all correspond to the S_1–S_0 transition.

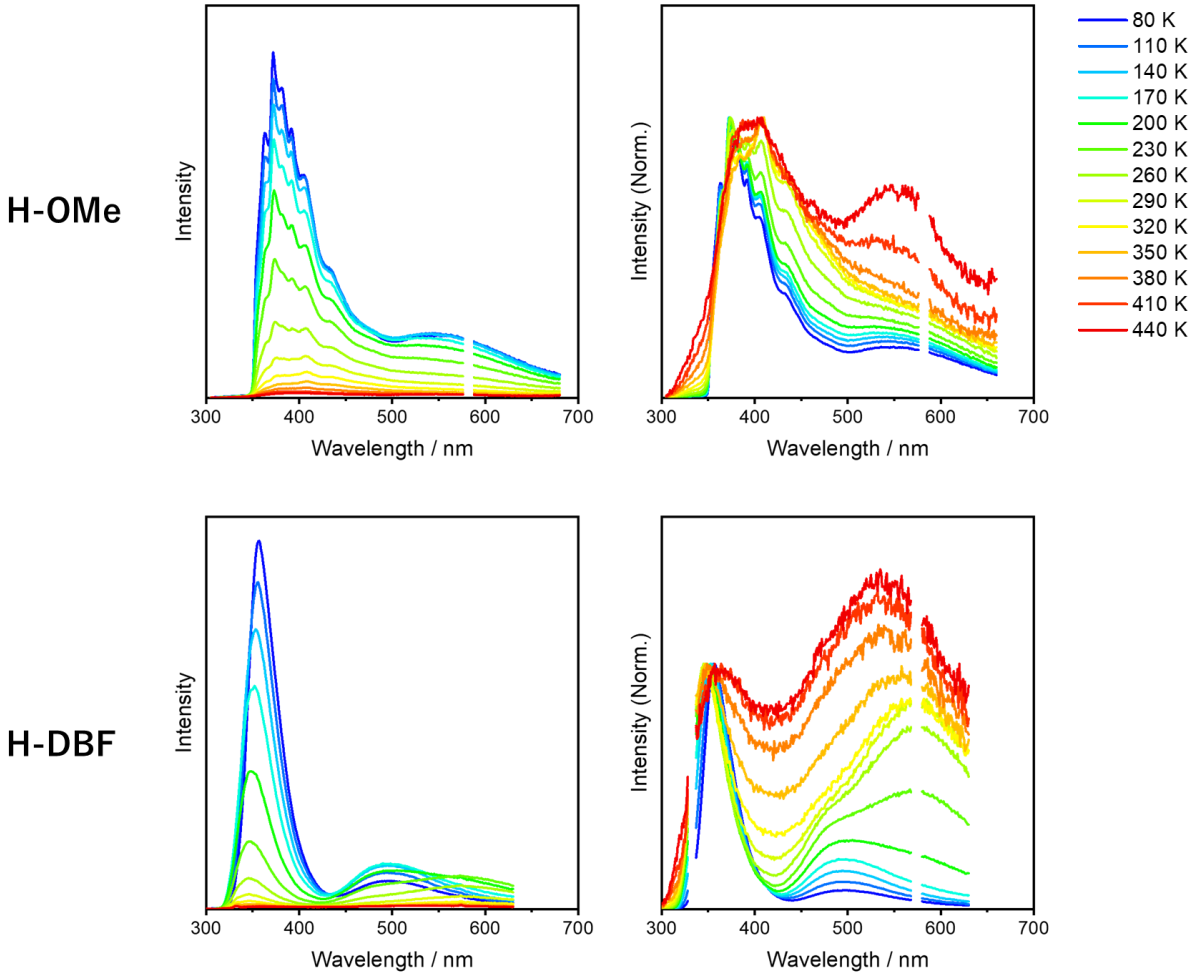

Figure 4. Variable temperature PL spectra of solid samples. Left column: raw stacked spectra. Right column: normalized spectra at the peak intensity of the LE emission.

Table of Contents

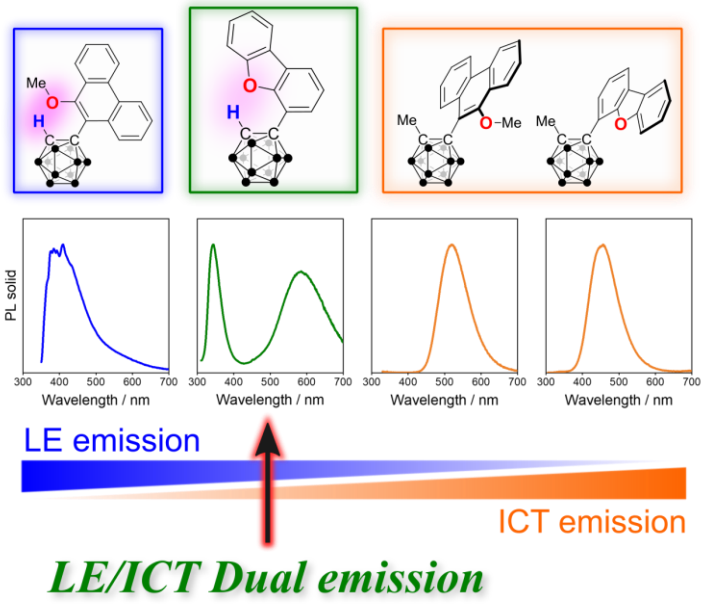

The dual-emission character of aryl-modified *o*-carboranes can be regulated by intramolecular CH···O interactions. Stronger interactions afforded a higher LE/ICT ratio due to the tightly locked molecular orientation favorable for LE emission. Well-balanced LE/ICT dual emission could be achieved by tuning intramolecular interaction sites in the solid state. The more activated molecular motions at higher temperature gradually perturbed LE/ICT ratio, resulting in the thermoresponsivity in solid.